Enhancing membrane performance for CO_2 capture from flue gas with ultrahigh MW polyvinylamine

Kai K. Chen, Yang Han, Zhien Zhang, W.S. Winston Ho*

William G. Lowrie Department of Chemical and Biomolecular Engineering and Department of Materials Science and Engineering, The Ohio State University, 151 West Woodruff Avenue, Columbus, OH 43210-1350, USA

* Corresponding author. Tel.: +1 614 292 9970; fax: +1 614 292 3769.

E-mail address: ho.192@osu.edu (W.S.W. Ho).

Abstract

Membranes for post-combustion CO_2 capture are required to have a high CO_2 permeance due to the limited driving force. For facilitated transport membranes synthesized with polyvinylamine (PVAm), a defect-free selective layer of <200 nm is usually required to render sufficient permeance with high CO_2/N_2 selectivity. In order to meet such a demand through the knife-coating process, the coating solution needs to have a high viscosity at a relatively low concentration to minimize its penetration into the substrate. The demand was met by synthesizing PVAm with an ultrahigh molecular weight (MW) via inverse emulsion polymerization (IEP) in this study. Compared to solution polymerization, IEP isolates the reaction in inverse micelles suspended in a continuous organic phase, which allows excellent dissipation of the heat generated by the reaction and reduces gel formation drastically. The polymerization parameters, including monomer concentration, initiator concentration, and reaction temperature, were investigated to obtain the optimal MW of PVAm for membrane performance. As compared to solution polymerization, IEP enhanced the MW of PVAm from 1.2 to 12.7 MDa, which minimized the penetration of the coating solution into the substrate and hence the extra mass transfer resistance. The effect of MW and degree of hydrolysis of PVAm on the membrane transport properties were studied. Furthermore, by employing PVAm with a MW of 12.7 MDa to strengthen the polymer matrix, the loading of piperazine glycinate in the membrane was increased up to 85 wt.%. The resultant membrane achieved a CO_2 permeance of 839 GPU and a CO_2/N_2 selectivity of 161 at the typical flue gas temperature of 57°C.

Keywords: CO_2 capture; Polyvinylamine; Facilitated transport membrane; Piperazine glycinate loading

1. Introduction

Among the carbon capture technologies for reducing the carbon emission from coal-fired power plants, membrane technology has the advantages of being compact, modular, energy-efficient, and easy to operate and maintain [1,2]. As the flue gas emitted by a typical coal-fired power plant has a large flow rate and a low CO_2 content balanced with mostly N_2 [3], membranes with both high CO_2 permeance and excellent CO_2/N_2 selectivity are required to achieve the target of >90% CO_2 capture with a CO_2 purity >95% set by the U.S. Department of Energy [4]. CO_2-selective polymeric membranes are promising candidates due to their low cost and ease of scale-up [5-14].

Amine-containing polymeric membranes have shown promising transport performances owing to the facilitated transport of CO_2 by the amino groups through selective and reversible reactions [5-7,9,15,16]. Specifically, polyvinylamine (PVAm) is a material of interest because of its high density of primary amino groups [6,12,17,18]. Robust CO_2-selective composite membranes can be synthesized by coating PVAm on a porous substrate (e.g., polyethersulfone) [19,20].

Kim et al. synthesized membranes with PVAm which had MWs ranging from 34 to 80 kDa, and found that a higher MW enhanced CO_2/CH_4 selectivity due to less chain mobility that significantly lowered the solution-diffusion transport of CH_4 [6]. Due to the lack of commercially available high-MW PVAm product, Chen et al. synthesized PVAm in-house through the solution polymerization of *N*-vinylformamide [12]. However, the polymerization method was limited by its poor heat and mass transfer when the reaction system became highly viscous. Also, autoacceleration could occur locally and cause gel formation, rendering the product unusable for membrane fabrication [21]. As a result, the MW of the PVAm obtained was limited at 1.2 MDa, which allowed a maximum mobile carrier loading of 65 wt.% [12].

In this study, inverse emulsion polymerization (IEP) was employed to further increase the MW of PVAm [22,23]. During the typical IEP (illustrated in Fig. 1), the aqueous monomer solution is dispersed in an organic phase, and the polymerization occurs in numerous dispersed polymer phases surrounded by the emulsifier molecules. Unlike solution polymerization, the heterogeneous reaction system of IEP allows the polymerization to occur within the isolated micelles rather than the hydrophobic continuous phase. Hence, the viscosity of the hydrophobic continuous phase does not change much. As better heat and mass transfer can be obtained for the reaction system, the chance of gel formation is significantly reduced.

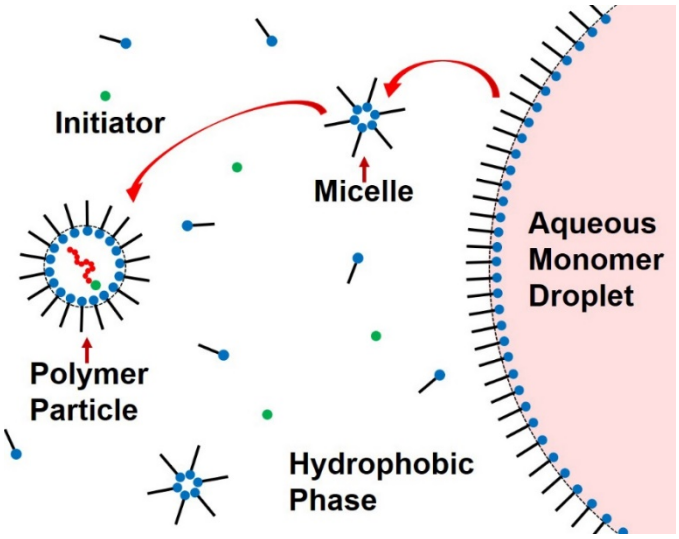

Fig. 1. Schematic of inverse emulsion polymerization.

As a higher MW of PVAm leads to a higher coating solution viscosity [24], the penetration of the coating solution into the porous substrate, and hence its resultant extra mass transfer resistance can be minimized or eliminated. Mobile carriers in the form of amino acid salt (e.g., piperazine glycinate) can also be blended into the PVAm matrix to enhance the membrane performance [12,25]. Furthermore, a higher MW gives a stronger polymeric matrix by creating more

entanglement of the polymer chains, resulting in a high viscosity even at a low polymer concentration. As a result, a desirable viscosity of the coating solution can be maintained for membrane coating even when a higher mobile carrier content is used. The polymerization conditions, including monomer concentration, initiator concentration, and reaction temperature, were investigated and optimized with respect to the MW of PVAm. The PVAm synthesized were characterized using viscometry, nuclear magnetic resonance (NMR), static light scattering (SLS), thermogravimetric analysis (TGA), and density measurement. Finally, composite membranes containing the synthesized PVAm were prepared, and their transport performances were investigated.

2. Experimental

2.1. Materials

N-vinylformamide (NVF, 98.5%) was donated by BASF SE (Ludwigshafen, Germany). It was purified by vacuum distillation at 40ºC. Glycine (99%), piperazine (99%), azobisisobutyronitrile (AIBN, 98%), sodium hydroxide (NaOH, 98%), and deuterium oxide (D_2O, 99.9%) were purchased from Sigma-Aldrich Corp. (Milwaukee, WI, USA). Sorbitan monostearate (Span® 60, 100%), toluene (99.5%), ethanol (90%), hydrochloric acid (HCl, Certified ACS Plus), and dialysis membrane tubings were bought from Fisher Scientific Inc. (Pittsburgh, PA, USA). *n*-Octane (98%) was acquired from VWR International (Radnor, PA, USA). A free sample of strong base anion exchange resin (Purolite® A600OH) was provided by Purolite Corp. (Bala Cynwyd, PA, USA).

2.2. PVAm synthesis with IEP

As shown in Fig. 2, free radical polymerization of NVF was first conducted to yield poly(*N*-vinylformamide) (PNVF) [18,26,27]. Instead of solution polymerization [18], the IEP technique

was employed in this study. Briefly, 1.5 g of Span® 60 was dissolved in 54 g of *n*-octane at 50°C inside a 500 mL three-neck reaction flask. Next, the purified NVF monomer was diluted to various concentrations with water, and 27 g of the prepared monomer solution was mixed with *n*-octane. The mixture was purged using nitrogen for 30 min to remove the dissolved oxygen before the temperature was raised to a target setting. Next, a predetermined amount of AIBN was dissolved in about 1 g of toluene and added into the reaction flask, marking the start of the reaction. The reaction proceeded for 1 h with vigorous stirring and a continuous nitrogen flow (10 cc/min) for protection. A condenser was fitted to the reaction flask to minimize the loss of solvent.

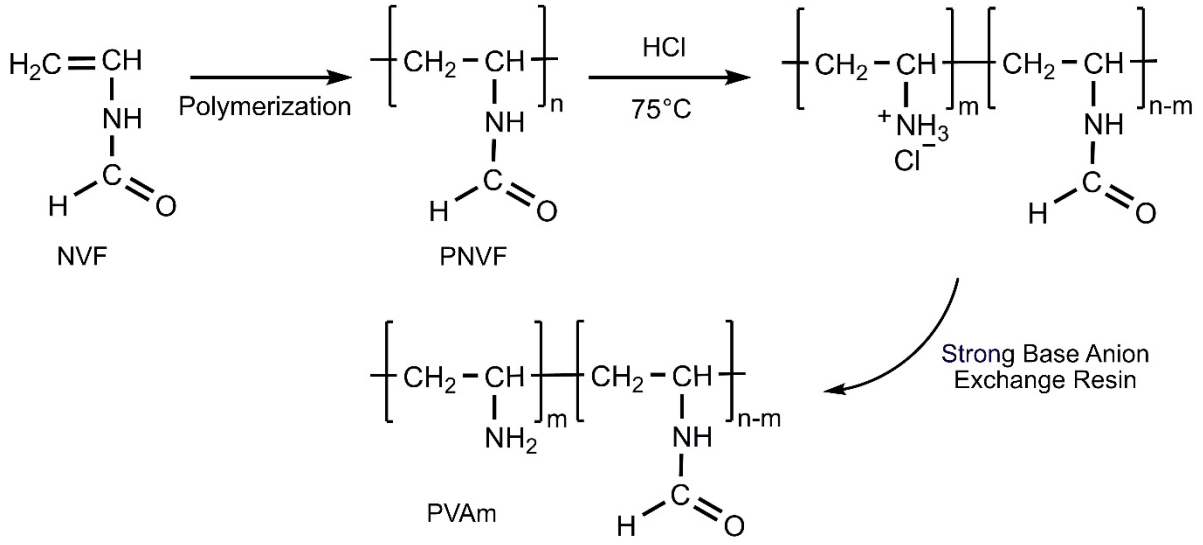

Fig. 2. Schematic of PVAm synthesis from NVF.

The reaction was terminated after 1 h by pouring the reaction mixture into an excess amount of ethanol for polymer precipitation. The precipitated PNVF solid appeared as a white powder, and the majority of the unreacted monomer was dissolved in ethanol. Subsequently, the PNVF solid was washed with ethanol and dried in a vacuum oven at 50°C for 12 h. The dried PNVF was then dissolved in water to make a 3.5 wt.% solution for acidic hydrolysis. Depending on the

targeted degree of hydrolysis, certain molar ratio of HCl to the amide groups in PNVF was used. The hydrolysis was carried out at 75°C for 5 h before the converted PVAm·HCl was precipitated in excess ethanol and dried in the vacuum oven. The solid was then dissolved in water to form a 2.5 wt.% solution for ion-exchange with strong base anion exchange resins until the pH reached 11.9. Finally, the PVAm solution was separated from the resins by vacuum filtration and was ready for preparing the membrane coating solution.

During the acidic hydrolysis step, the electrostatic repulsion between the protonated amino groups and the hydronium ions shields some amide groups from being reacted [28], prohibiting a complete conversion. In order to achieve a 100% degree of hydrolysis, basic hydrolysis was conducted with NaOH. The ratio of NaOH/amide used was 2:1, and the reaction was carried out at 75°C for 5 h [27]. Since the PVAm obtained had a high pH, it could not precipitate in ethanol. Thus, dialysis was carried out by enclosing the reaction product in a dialysis tubing (4 nm pore size), which was placed in deionized water with a 50× equivalent volume [29]. The dialysis tubing allowed sodium formate to diffuse out while retaining the PVAm within. The deionized water was under constant agitation and was replaced every 6 h for one day.

2.3. Characterization of PVAm

The NMR samples were prepared by dissolving the PVAm solid in D_2O with a concentration of 1 wt.%. ^{1}H-NMR was obtained by a 400 MHz AVANCE™ III HD system (Bruker Corporation, Billerica, MA, USA). In addition to confirming the identity of PVAm, the conversion of the hydrolysis step was quantified by calculating the degree of hydrolysis (DOH), which is defined as [27]:

$$\mathrm{DOH} = \left(1 - \frac{2 \times \text{amide group peak area}}{\text{methylene group peak area}}\right) \times 100\% \qquad (1)$$

where the peak areas of the specified functional groups can be measured by integrating the corresponding NMR peaks using Bruker's TopSpin™ software.

The shear viscosities of the coating solutions were measured with a Brookfield Digital Viscometer DV-E (Brookfield Engineering Laboratories, Inc., Middleboro, MA, USA). Additionally, the intrinsic viscosity of each PVAm sample was also measured by the viscometer. First, the polymer solution was diluted to obtain five samples with concentrations of 0.1, 0.2, 0.3, 0.4, and 0.5 wt.%, respectively. The shear viscosities of these samples were measured, and the relative and reduced viscosities were calculated to extrapolate the intrinsic viscosity [30].

The weight-average MWs of the PNVF samples were characterized by the SLS technique. Details of the procedure have been included in the Supporting Information (SI). With the known MW of a given PNVF sample, the MW of a corresponding PVAm sample was estimated by the DOH of PVAm, assuming the polymer chain length had not been affected by the hydrolysis reaction. By using the MWs of the PNVF and PVAm repeating units being 71 and 43 Da, respectively, the MW of the obtained PVAm ($\mathrm{MW_{PVAm}}$) can be derived from the MW of the corresponding unhydrolyzed PNVF ($\mathrm{MW_{PNVF}}$) as follows:

$$\mathrm{MW_{PVAm}} = \mathrm{MW_{PNVF}} \times \frac{71 \times (1 - \mathrm{DOH}) + 43 \times \mathrm{DOH}}{71} \tag{2}$$

The fractional free volume (FFV) of free-standing membrane samples was determined as follows [1]:

$$\mathrm{FFV} = \frac{V - V_0}{V} \tag{3}$$

where V is the measured specific volume of membrane sample, which can be calculated as the inverse of the membrane density, and V_0 is the specific core volume of the membrane components,

which can be calculated based on the group contribution method [31,32]. Details of the characterization procedure can be found in the SI.

TGA was done with a Cahn TherMax 500 TGA system (Thermo Fisher Scientific, Waltham, MA, USA). The temperature changed from 50 to 600ºC with a heating rate of 10ºC/min. Moreover, the absorbance of the coating solution was measured by a UV–Vis spectrophotometer (UV-1700, Shimadzu, Japan) at a wavelength of 550 nm. RO water was used as the reference for calibration.

2.4. Composite membrane synthesis

The preparation of the piperazine glycinate (PG) solution was detailed in the previous study [12]. Briefly, glycine was first dissolved in water to form a 17.5 wt.% solution. Next, an equimolar amount of piperazine was added to the glycine solution under continuous mixing until a homogeneous PG solution was obtained. The coating solution was synthesized by blending the PG and PVAm solutions at a specified ratio. If necessary, the coating solution was concentrated by nitrogen purging to achieve a desirable viscosity. The polymer content in the coating solution was controlled at 2 wt.% for all the compositions presented in this study.

Next, the PVAm/PG solution was coated on a PES substrate (average pore size = 35 nm) prepared in-house [19]. A Digital Micron II Film Applicator from Gardco Inc. (Pompano Beach, FL, USA) equipped with an adjustable gap setting with a precision of 1 μm was used for the coating, which was carried out at a constant gap setting of 15 μm and a coating speed of about 2 cm/s [18]. Finally, the membrane was dried in a fume hood overnight.

2.5. Characterization of composite membranes

The gas transport performance of the composite membrane was measured in a transport measurement unit [12]. The schematic of the unit has been shown in our previous study [12]. In brief, the feed gas was a mixture of CO_2/N_2 (20/80 by volume) at a flow rate of 60 cc/min, and an

argon stream at 30 cc/min was used as the sweep gas. The feed and permeate pressures were set at 1.5 and 1.1 psig, respectively. The test was conducted at 57ºC, and the effective membrane area was 2.7 cm^2. The feed and sweep gases were fully saturated at 57ºC. Gas samples of retentate and permeate were dried with water knockout vessels and analyzed by an Agilent 6890N gas chromatography (GC, Agilent Technologies, Palo Alto, CA, USA).

The tested membranes were cut into thin stripes before immersed in liquid nitrogen and fractured to obtain clean cross-sections. Scanning electron microscopy (SEM, FEI Apreo LoVac High Resolution, ThermoFisher Scientific, Waltham, MA, USA) and the ImageJ software (National Institutes of Health, USA) were utilized to quantify the thickness of the selective layer [20,33,34].

3. Results and discussion

3.1. Mark-Houwink equation for PNVF

MW measurement via the SLS technique was conducted frequently in this study. However, since the SLS procedure was time-consuming, it was desirable to obtain a Mark-Houwink equation that correlated the polymer's MW to its intrinsic viscosity, for which the measurement was easier compared with the SLS experiments. Herein, the Mark-Houwink equation of PNVF was determined. Moreover, after the MW of a PNVF sample has been determined, the MW of the corresponding PVAm can be calculated using Eq. (2) with a known DOH.

Before the measurement of the weight-average MW was conducted, the refractive index increment (dn/dc) of each polymer sample was obtained with a deflection type refractometer. The dn/dc values of the PNVF samples had an average value of 0.1845 mL/g. Next, the dn/dc value

was applied to the SLS measurement. A Berry plot was generated for each sample in the accompanying software of the goniometer system, and an example of the plot is included in SI.

In order to establish the equation, PNVF samples synthesized with different IEP conditions were characterized for their MWs and intrinsic viscosities, respectively. The data are presented in the Mark-Houwink plot shown in Fig. 3.

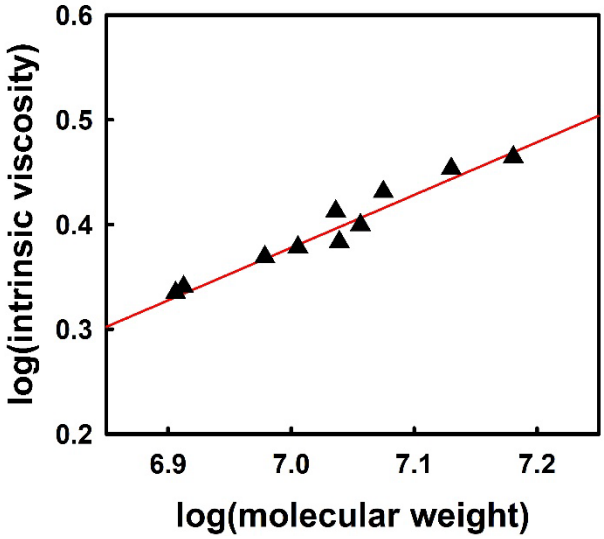

Fig. 3. Mark-Houwink plot of PNVF synthesized with IEP.

As seen in the log-log plot, the data points display a linear trend. The Mark-Houwink equation obtained from the fitting is:

$$[\eta] = 7.11 \times 10^{-4} {M_W}^{0.5037} \quad (4)$$

where $[\eta]$ is the intrinsic viscosity in dL/g and M_W is the weight-average MW in Da. The power value of 0.5037 indicates that water is a good solvent for the polymer. A previous study has also obtained a Mark-Houwink relationship for PNVF [30], but the range of MW investigated was limited within 0.1–0.9 MDa. Hence, this study was complementary to the previous study by extending the MW in the range of 5–15 MDa.

3.2. Optimization of IEP conditions for ultrahigh MW PVAm

The synthesis conditions of IEP were optimized in order to obtain the PNVF and its corresponding PVAm with the highest possible MW. The effects of monomer concentration, initiator concentration, and reaction temperature on the MW were investigated, respectively.

Fig. 4 shows the effect of monomer concentration on the MW of PNVF. An initiator concentration of 0.019 wt.% was used, and the reaction temperature was maintained at 70ºC. As the monomer concentration in the aqueous phase was increased from 30 to 42.5 wt.%, the MW was increased from 9.5 to 15.2 MDa. Such a phenomenon was expected since a higher monomer concentration led to a faster rate of polymerization, making the average polymer chain length longer. An attempt was also made to increase the monomer concentration even higher (i.e., 45 wt.%). However, gel particles were observed in the reaction product, indicating that the monomer concentration was too high to have a controlled polymerization.

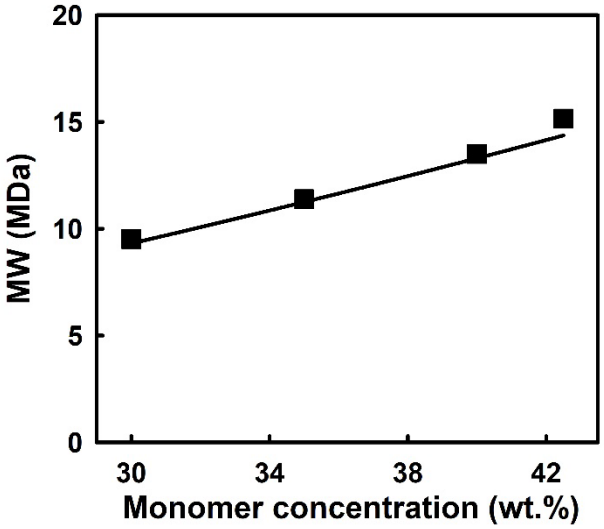

Fig. 4. Effect of monomer concentration on MW of PNVF. 0.019 wt.% initiator and 70ºC reaction temperature.

Fig. 5 illustrates the effect of initiator concentration on the MW of PNVF. It shows an opposite trend to that of Fig. 4. The monomer concentration was kept at 42.5 wt.%, and the reaction temperature used was 70ºC. As the initiator concentration in the reaction mixture was varied from 0.019 to 0.022 wt.%, the MW was reduced from 13.5 to 8.2 MDa. This could be due to the faster termination of the polymer chain propagation and shortened the average polymer chain length [21]. It should be noted that an initiator concentration lower than 0.019 wt.% was not practical, since the insufficient amount of initiator would result in a low polymer yield.

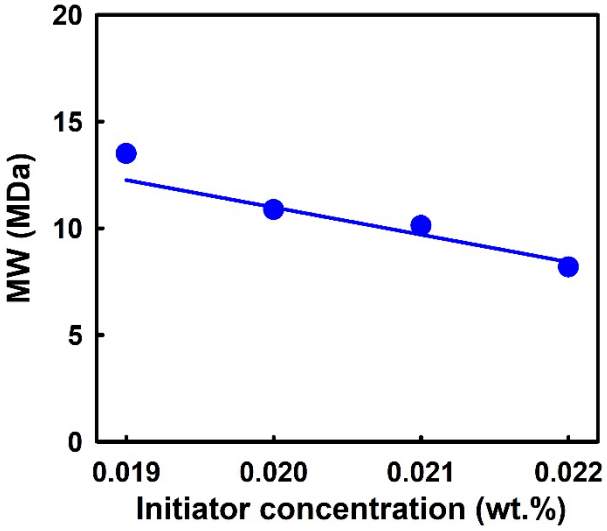

Fig. 5. Effect of initiator concentration on MW of PNVF. 42.5 wt.% monomer and 70ºC reaction temperature.

Lastly, the effect of reaction temperature on the MW of PNVF was investigated (Fig. 6), in which the monomer and initiator concentrations were kept at 42.5 and 0.019 wt.%, respectively. As seen in Fig. 6, an optimal temperature was observed at 70ºC, where the MW was at 13.5 MDa. The temperature affected the polymer chain length in two ways. On one hand, a higher temperature caused a higher rate of polymerization, which led to a longer average polymer chain. On the other hand, a higher temperature also promoted the dissociation of the initiator, and it was shown earlier that a higher concentration of free radicals resulted in a lower MW. Hence, as the temperature increased from 65 to 70ºC, the faster rate of polymerization outweighed the effect of the faster rate of initiator dissociation, and a longer average polymer chain length was obtained. As the temperature was increased beyond 70ºC, the effect of the higher free radical concentration dominated and resulted in shorter polymer chains. The polymerization conditions and the corresponding MW and $[\eta]$ are summarized in Table S1 in the SI.

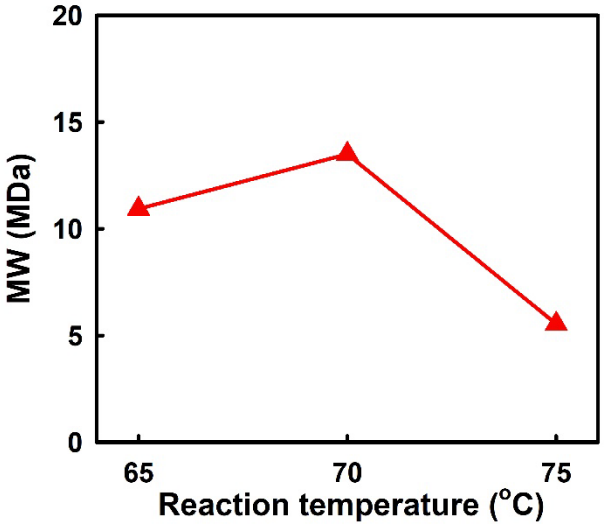

Fig. 6. Effect of reaction temperature on MW of PNVF. 0.019 wt.% initiator and 42.5 wt.% monomer.

It is expected that the temperature control of a scaled-up polymerization process should not be a problem owing to the following. The inverse emulsion system uses a low viscosity of the continuous organic phase for a thorough mixing and fast heat transfer, eliminating local temperature spikes. Also, process design with online temperature monitoring can keep the temperature variation within ±0.5ºC [35], which is narrow enough for a controlled reaction.

It should be noted that, when the polymerization occurred for 1 h at the conditions of 42.5 wt.% monomer, 0.019 wt.% initiator and 70ºC, the conversion of the monomer was about 80%. Even though the effect of reaction time was not studied, it is expected that a longer reaction time will lead to a higher conversion. However, a longer reaction time would also lead to a lower weight-average MW since additional polymer chains formed would be shorter as the monomer

concentration continues to decrease [36]. Because a high MW and a decent conversion had been achieved in this work, a longer reaction time was not pursued.

3.3. DOH and thermal analysis of PVAm

The synthesized PNVF was converted into PVAm·HCl through acidic hydrolysis with HCl [12]. Fig. 7 shows the ^{1}H NMR spectra of (a) PNVF and (b) PVAm·HCl, respectively. The peaks were assigned to different hydrogen atoms of the polymer [27,28,37-40]. In particular, the peaks around 2 ppm were assigned to the methylene groups, and the peaks around 8 ppm should represent the amide groups. Furthermore, the peak of the amino groups could not be observed because of rapid hydrogen exchanges between the amino groups and the D_2O solvent. The sharp peak at around 4.8 ppm was identified as HDO, and both the peaks at around 1.2 and 3.7 ppm were caused by the residual ethanol present in the polymer. As illustrated by the chemical structures shown in the figure, some amide groups in PNVF were converted into protonated amino groups as in the PVAm·HCl after the acidic hydrolysis. As explained earlier, the incomplete conversion was due to the electrostatic repulsion between the protonated amino groups and hydronium ions. By employing Eq. (1), the DOH can be calculated to quantify the conversion.

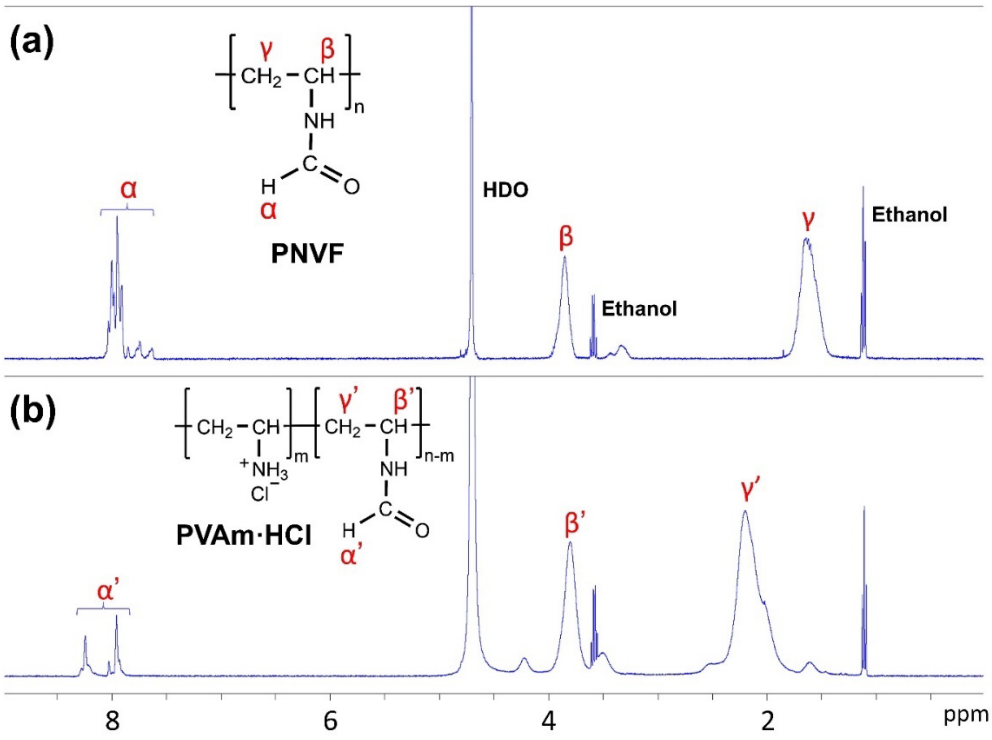

Fig. 7. NMR spectra of (a) PNVF and (b) PVAm·HCl.

Fig. 8 demonstrates the effect of the HCl/amide molar ratio for the acidic hydrolysis on the DOH of PVAm. The hydrolysis duration was kept at 5 h, and the temperature used was 75ºC. As the HCl/amide ratio was varied from 0.1 to 2.0, the DOH increased from 4.8 to 80.1%. At the HCl/amide ratio of 2, the rising trend of DOH started to plateau out. It should be noted that a higher DOH can still be achieved with acidic hydrolysis under harsher conditions. For instance, an experiment was conducted with a HCl/amide ratio of 3 for 5 h at 85ºC, and the resultant polymer had a DOH of 94.4%. Since the harsher conditions of acidic hydrolysis gave a diminishing return on additional DOH increase, the basic hydrolysis method is recommended for obtaining a DOH above 80% [27]. However, it is not preferred due to the extended duration of the dialysis step required to purify the PVAm solution after the hydrolysis. Nonetheless, one batch of PVAm with

100% DOH was prepared for the membrane transport parametric study with respect to DOH. It should be noted that, by knowing the MW of a PNVF and the DOH of the PVAm obtained after hydrolyzing the PNVF, the MW of the PVAm can be determined using the MW correlation presented in Eq. (2). In order to provide a guidance for designing future acidic hydrolysis reactions, the data was fitted with a quadratic relationship displayed in Fig. 8.

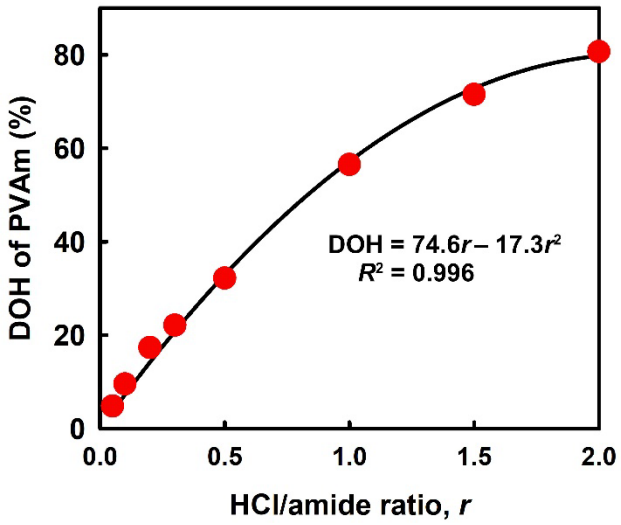

Fig. 8. Effect of HCl/amide ratio on the DOH of PVAm at 75ºC.

Subsequently, strong base anion exchange resins were employed to raise the pH of the PVAm solution to 11.9. Free-standing films were prepared from PVAm with a DOH of 15% and a MW of 12.7 MDa, and the film was subjected to TGA analysis. The reason for choosing this PVAm sample was because it was shown, as elaborated in the later sections, to give the optimal membrane transport performance. The TGA data and the corresponding derivative thermogravimetric (DTG) curve are displayed in Fig. 9. First, 5% weight loss of the sample was experienced at 168ºC mainly due to water desorption, which could be attributed to the gradual release of bound water that interacted strongly with the hydrophilic PVAm via hydrogen bond and electrostatic forces

[41,42]. Two major stages of weight reduction began at around 200 and 350ºC, respectively, and they should be the results of the release of ammonia and hydrazine during the polymer decomposition [43].

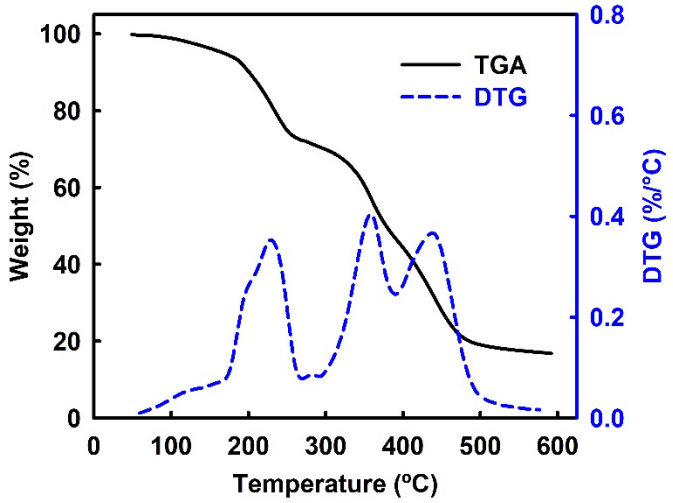

Fig. 9. TGA and DTG curves of PVAm with MW of 12.7 MDa.

3.4. Effect of PVAm MW on transport properties of neat PVAm membranes

Coating solutions (2 wt.%) of PVAm with MWs ranging from 5.2 to 14.3 MDa were prepared; the DOH was kept at 15%. Neat PVAm membranes were coated on the PES support, and their transport performances are shown in Fig. 10. As seen in the figure, when the MW was increased from 5.2 to 12.7 MDa, the CO_2 permeance was enhanced from 410 to 510 GPU. Meanwhile, the N_2 permeance became slightly higher as well, and hence the CO_2/N_2 selectivity experienced a minor drop from 50 to 48. However, the CO_2 permeance and CO_2/N_2 selectivity dropped to 472 GPU and 42, respectively, as the MW was raised further to 14.3 MDa.

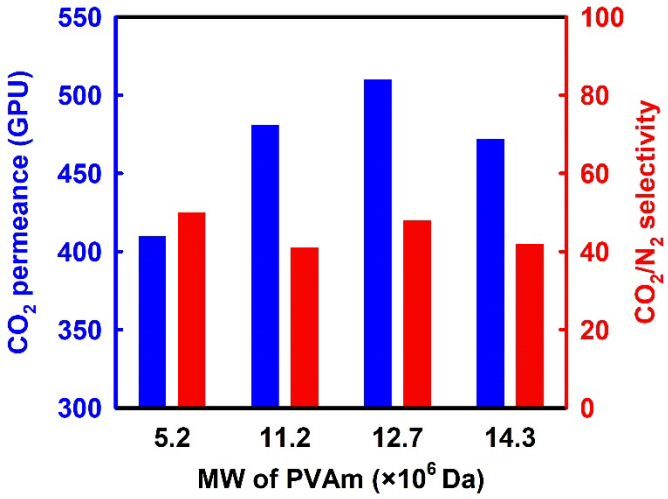

Fig. 10. Effect of PVAm MW on transport performances of neat PVAm membranes.

The performance improvement up until the MW of 12.7 MDa could be explained by the higher viscosity of the coating solution synthesized. As illustrated in Fig. 11, the viscosity of the coating solutions increased almost linearly from 917 to 1379 cp as the PVAm MW increased from 5.2 to 12.7 MDa. The thicknesses of the corresponding membranes determined from their cross-sectional SEM images (Fig. S2 in SI) reduced gradually from 149 to 138 nm. In addition to the reduction in the selective layer thickness, it is likely that the coating solution also penetrated less into the substrate. As a result, the effective thickness of the selective layer was lower, making the membrane more permeable.

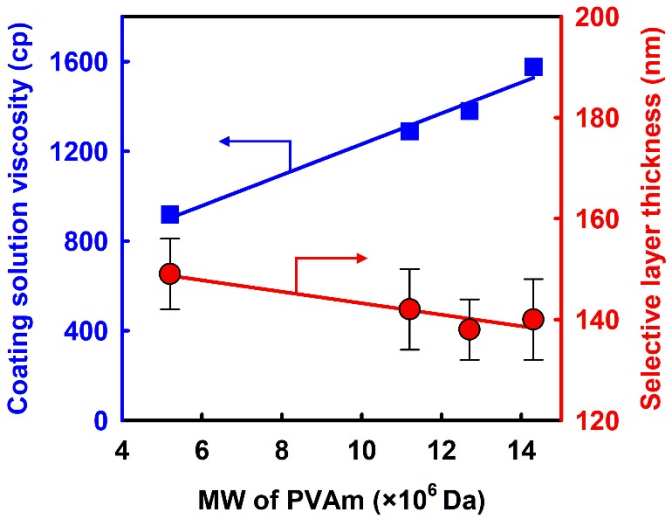

Fig. 11. Effect PVAm MW on coating solution viscosity and thickness of selective layer. The trendlines are for the guide of eyes.

It is noted that studies have shown that the coating thickness obtained from the knife-coating method is related to the capillary number $Ca = \eta v/\rho$, where η is the solution viscosity, v the coating speed, and ρ the density of the coating solution [44,45]. In the study of Berre et al. [44], as the coating speed increased (resulting in a higher Ca), the coating thickness reduced initially (evaporation regime), reached a minimum, and increased afterwards (Landau-Levich regime). Similarly, in this study shown in Fig. 11, as the viscosity increased (also corresponding to an increasing Ca), the membrane thickness reduced slightly and reached a plateau with increasing viscosity. The data might indicate the transition from the evaporation to the Landau-Levich regime, with the minimum thickness obtained at the viscosity of around 1400 cp.

Moreover, in Kim et al.'s study with PVAm, an increase in the PVAm MW from 20 to 80 kDa significantly enhanced the CO_2/CH_4 selectivity [6]. However, the trend was not observed in the present study presumably because the membrane thickness became thinner, which usually results

in a lower selectivity [46], as the PVAm MW increased. Besides, the difference in the kinetic diameters between CO_2 and CH_4 (0.5 Å) is larger than that between CO_2 and N_2 (0.34 Å) [1,47], which could have made the CO_2/CH_4 selectivity more sensitive to the tighter membrane matrix at higher PVAm MW.

Furthermore, the reduction of the membrane transport performance at the MW of 14.3 MDa could be explained by the inhomogeneity discovered in the coating solution, which is described in the following. Fig. 12 shows the absorbance values of the PVAm coating solutions at different MWs measured by UV–Vis at the wavelength of 550 nm. As the MW increased from 5.2 to 12.7 MDa, the absorbance increased slightly from 0.223 to 0.315. It was followed by a drastic increase to 0.492 at the MW of 14.3 MDa. The exponential increase in the absorbance could be a result of the formation of invisible gel particles during the synthesis. Since the polymer with 14.3 MDa was synthesized at a relatively high monomer concentration (42.5 wt.%) and a considerably low initiator concentration (0.019 wt.%), the fast rate of polymerization could result in microscopic gel formation, which would hinder the gas transport through the membrane. Also, the relatively high reaction temperature at 70ºC increased the risk of autoacceleration of the polymerization [21]. Better control of the reaction could be achieved by using an initiator that requires a lower dissociation temperature.

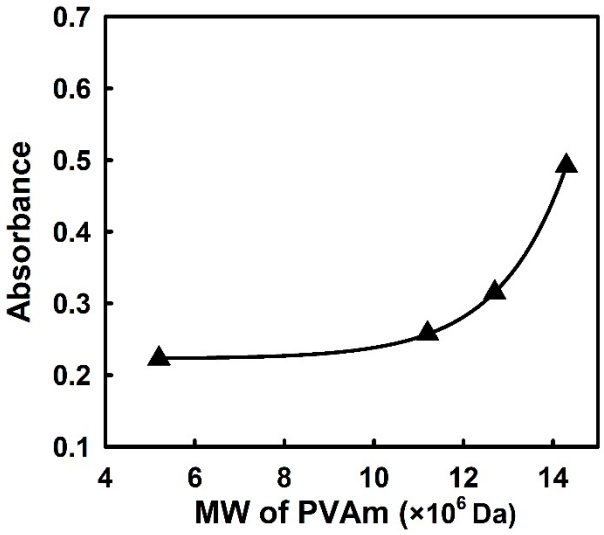

Fig. 12. UV–Vis absorbance of 2 wt.% PVAm polymer solutions with different MWs. The trendline is for the guide of eyes.

In addition, insufficient evidence was available to analyze the effect of MW on the CO_2 permeability of the selective layer. Since the penetration depth of the selective-layer material into the substrate was unknown, the CO_2 permeance of the selective layer could not be calculated using the resistance-in-series model [19]. Besides, although a study on thick polyimide membranes (40–70 μm) reported that the CO_2 permeability became higher with increasing MW [48], the study could not confirm the cause of the permeability increase. Also, the same effect may not apply to ultrathin membranes (<150 nm) that were studied in this work, particularly for the thin facilitated transport membranes that the permeability may not be a useful indicator.

3.5. Effect of the DOH of PVAm on membrane transport properties

The effect of the DOH of PVAm on the transport performances of neat PVAm membranes is illustrated in Fig. 13. As the DOH increased from 15% to 99.5%, the CO_2 permeance was enhanced from 362 to 524 GPU, owing to a higher content of the amino groups that served as the

fixed-site carriers. Meanwhile, the CO_2/N_2 selectivity increased from 29 to 38, which was mainly due to the higher CO_2 permeance.

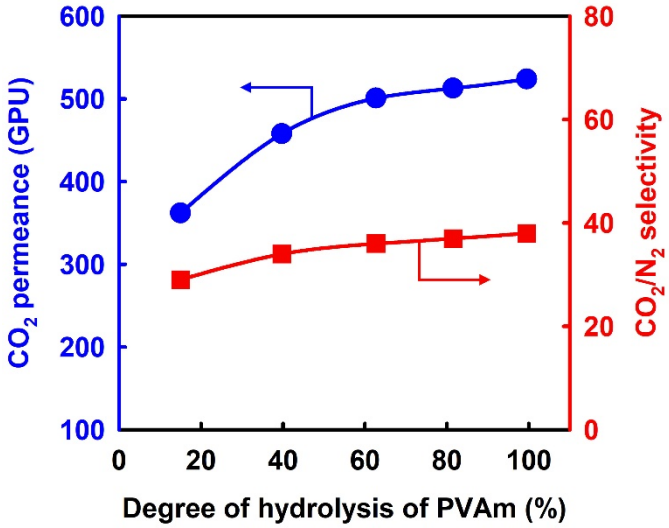

Fig. 13. Effect of the DOH of PVAm on transport performances of neat PVAm membranes. The trendlines are for the guide of eyes.

Next, 65 wt.% of PG was incorporated into the membrane balanced with PVAm. As depicted in Fig. 14, the best performance occurred at around 15% DOH of PVAm, with a CO_2 permeance of 830 GPU and a CO_2/N_2 selectivity of 161. Compared with the neat PVAm membranes, the significantly enhanced CO_2 permeance was due to the higher diffusivity of the mobile carrier. The better CO_2/N_2 selectivity was mainly because of the higher CO_2 permeance. Moreover, the hydrophilic nature of the mobile carrier also retained more water in the membrane and lowered the solubility of the nonpolar N_2 [49].

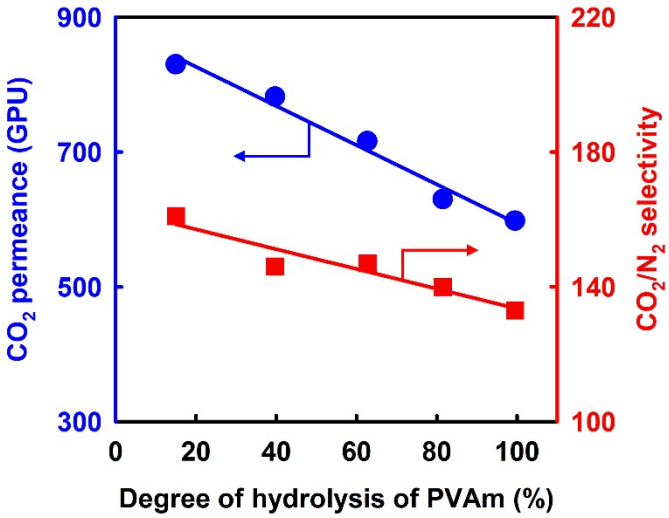

Fig. 14. Effect of the DOH of PVAm on transport performances of PVAm/PG (35/65 by wt.) membranes. The trendlines are for the guide of eyes.

As depicted in Fig. 14, with an increasing DOH, the transport properties of the membranes containing 65 wt.% PG demonstrated a dropping trend. Specifically, at the DOH of 99.5%, the membrane showed a CO_2 permeance of 598 GPU and a CO_2/N_2 selectivity of 133. The trend was unlikely to be caused by variation in the membrane water absorption. At 57ºC and 100% relative humidity, Deng et al. [49] demonstrated that the water uptake levels of neat PVAm and membranes containing 85 wt.% mobile carriers (2-(1-piperazinyl)ethylamine sarcosinate) were 75.4% and 233.2%, respectively. It signaled that PVAm contributed less to the water uptake as compared to the mobile carriers. Hence, the DOH variation of PVAm should not affect the membrane water uptake significantly.

The reduction in the transport performance could partly be explained by the reduced FFV of the membrane matrix. Fig. 15 shows the effect of the DOH of PVAm on the measured specific volume (V), calculated specific core volume of the membrane components (V_0), and FFV of the

free-standing PVAm/PG (35/65 by wt.) membranes, respectively. First, V was obtained by measuring the density of each membrane sample and calculating the inverse of the density. The variation of the data measured at each DOH was within 0.2%. As seen in this figure, when the DOH increased from 15% to 62.7%, the measured specific volume first reduced from 0.752 cm^3/g to a minimum of 0.730 cm^3/g. Afterwards, V increased to reach 0.741 cm^3/g at a DOH of 99.5%. It should be noted that, even though the calculated core volume of each mole of the amide group (42.1 cm^3/mol) is higher than that of the amino group (26.6 cm^3/mol), the specific core volume V_0 of the amide group (0.592 cm^3/g) is smaller than that of the amino group (0.616 cm^3/g) after considering their respective MWs [31,32]. Hence, the calculated specific core volume of the membrane components V_0 increased from 0.707 to 0.716 cm^3/g as the DOH increased from 15% to 99.5%.

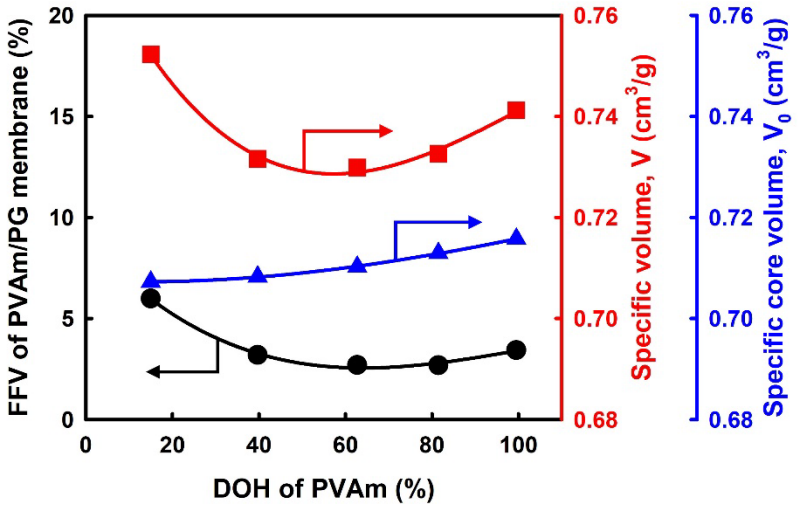

Fig. 15. Effect of the DOH of PVAm on V, V_0, and FFV of PVAm/PG (35/65 by wt.) membranes. The trendlines are for the guide of eyes.

As a result, the FFV of the free-standing membranes reduced from 5.98% to 3.43% as the DOH increased from 15% to 99.5%, with the FFV at 15% DOH being the highest. A higher FFV would allow the product of CO_2–amine reaction to diffuse through the membrane at a higher rate. Although more fixed-site amino groups were present at a higher DOH, the higher diffusivity enabled by the higher FFV at the lower DOH benefited the membrane performance more.

It is acknowledged that a more representative characterization of the membrane free volume should be conducted with samples equilibrated at 57ºC and 100% relative humidity, which were the conditions used for the membrane transport measurement. Other techniques for free volume measurement, such as positron annihilation lifetime analysis, could be employed in the future. Nonetheless, the FFV data of dry membranes offer one perspective of how the DOH of PVAm could have affected the membrane transport, as the higher FFV (Fig. 15) corresponded to better membrane transport results (Fig. 14) at the lower DOH.

3.6. Improved mobile carrier loading with ultrahigh MW PVAm

Subsequently, since the PVAm with a higher MW also provides a stronger polymer matrix, a higher mobile carrier content could be incorporated to improve the transport performance of the membrane. In the previous study that the synthesized PVAm with a low MW using solution polymerization [18], the amount of PG integrated into the selective layer was constrained at 65 wt.%. It was because the membranes synthesized with higher PG contents showed unstable transport performances, which was due to a weak polymer matrix that could not hold the mobile carrier in place.

The transport properties of the membranes with higher PG contents are shown in Fig. 16. It is worth noting that, since PVAm was the key component in the coating solution to provide the high viscosity, the PVAm concentration in the solution was kept constant at 2 wt.% for all the

compositions. As the PG concentration was increased from 65 to 85 wt.%, the CO_2 permeance improved from 774 to 839 GPU. Meanwhile, the CO_2/N_2 selectivity was maintained at around 165. There was a slight reduction in the selectivity from 172 to 161 as the PG content increased from 75 to 85 wt.%. It could be due to the lowered PVAm content that resulted in a looser membrane matrix for faster N_2 diffusion. Nonetheless, all membranes exhibited stable performances for at least 24 h, signaling that the PVAm matrix was able to hold a PG content of as high as 85 wt.%. The membrane demonstrated better stability than that synthesized with a low MW PVAm (0.72 MDa) and 70 wt.% of mobile carrier in our previous study, which recorded a performance degradation within 12 h [18]. A PG content higher than 85 wt.% is not recommended since a reduced polymer content in the membrane matrix may lead to a looser membrane matrix and hence a lower selectivity.

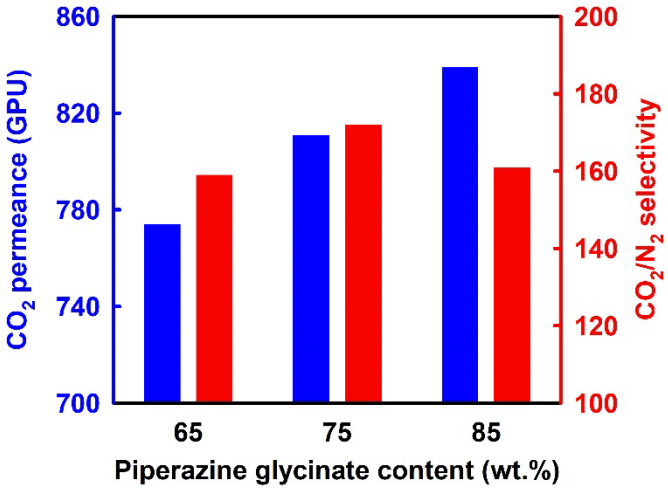

Fig. 16. Effect of PG content on membrane transport performances.

4. Conclusions

PVAm samples with ultrahigh MWs were successfully synthesized via IEP. As compared to the solution polymerization method, IEP allowed better control and avoidance of gel formation and enhanced the MW of the PVAm from 1.2 to 12.7 MDa. A higher MW (up to 12.7 MDa) led to an improved transport performance owing to a reduced selective layer thickness and less penetration into the substrate. Subsequently, a higher DOH of PVAm benefited the transport performance of the neat PVAm membranes due to a higher amine content in the membrane to facilitate the CO_2 transport. However, after PG was added into the membrane as the mobile carrier, the optimal membrane performance was obtained at a DOH of 15%, which was due to the higher FFV at this DOH, thus a higher diffusivity of the mobile carrier. Furthermore, the PVAm with a MW of 12.7 MDa provided a stronger polymer matrix and allowed the content of PG to be increased from 65 to 85 wt.%. The 85 wt.% PG membrane showed an improved performance with a CO_2 permeance of 839 GPU and a CO_2/N_2 selectivity of 161 at 57ºC.

Acknowledgments

We would like to thank Isaac Andy Aurelio, Katharina Daniels, José D. Figueroa, Krista Hill, and David Lang of the U.S. Department of Energy - National Energy Technology Laboratory (DOE-NETL) for their invaluable inputs and helpful discussions for this work. The SEM was performed at the Center for Electron Microscopy and Analysis (CEMAS) at The Ohio State University. We appreciate the donations of *N*-vinylformamide and Ultrason® E7020P PES from BASF Corporation (Ludwigshafen, Germany and Charlotte, NC) and the Purolite® A600OH resins from Purolite Corporation (Bala Cynwyd, PA). We gratefully acknowledge the funding from DOE/NETL (DE-FE0026919, DE-FE0031635, and DE-FE0031731) and the Ohio Development

Services Agency (OER-CDO-D-15-09, OER-CDO-D-19-12, and OER-CDO-D-19-13). This work was partly supported by the Department of Energy under Award Number DE-FE0026919 with substantial involvement of the National Energy Technology Laboratory, Pittsburgh, PA, USA.

Nomenclature

Ca	capillary number
M_W	weight-average molecular weight (Da)
$\mathrm{MW_{PNVF}}$	molecular weight of poly(*N*-vinylformamide)
$\mathrm{MW_{PVAm}}$	molecular weight of polyvinylamine
r	HCl/amide ratio
V	measured specific volume of membrane sample (cm^3/g)
V_0	calculated specific core volume of the membrane components (cm^3/g)

Greek letters

ρ	density of coating solution (g/ml)
η	solution viscosity (dL/g)
$[\eta]$	intrinsic viscosity (dL/g)
υ	coating speed for membrane coating (cm/s)

References

[1] W.S.W. Ho, K.K. Sirkar, Membrane Handbook, Champan & Hall, New York, 1992, Kluwer Academic Publishers, Boston, reprint edition, 2001.

[2] S.D. Kenarsari, D. Yang, G. Jiang, S. Zhang, J. Wang, A.G. Russell, Q. Wei, M. Fan, Review of recent advances in carbon dioxide separation and capture, RSC Advances 3 (2013) 22739–22773.

[3] T.C. Merkel, H. Lin, X. Wei, R. Baker, Power plant post-combustion carbon dioxide capture: An opportunity for membranes, J. Membr. Sci. 359 (2010) 126–139.

[4] K. Ramasubramanian, H. Verweij, W.S. Winston Ho, Membrane processes for carbon capture from coal-fired power plant flue gas: A modeling and cost study, J. Membr. Sci. 421–422 (2012) 299–310.

[5] H. Matsuyama, A. Terada, T. Nakagawara, Y. Kitamura, M. Teramoto, Facilitated transport of CO_2 through polyethylenimine/poly(vinyl alcohol) blend membrane, J. Membr. Sci. 163 (1999) 221–227.

[6] T.J. Kim, B.A. Li, M.B. Hägg, Novel fixed-site-carrier polyvinylamine membrane for carbon dioxide capture, J. Polym. Sci. Pol. Phys. 42 (2004) 4326–4336.

[7] J. Zou, W.S.W. Ho, CO_2-selective polymeric membranes containing amines in crosslinked poly(vinyl alcohol), J. Membr. Sci. 286 (2006) 310–321.

[8] D. Aaron, C. Tsouris, Separation of CO_2 from flue gas: A review, Sep. Sci. Technol. 40 (2005) 321–348.

[9] J. Huang, J. Zou, W.S.W. Ho, Carbon dioxide capture using a CO_2-selective facilitated transport membrane, Ind. Eng. Chem. Res. 47 (2008) 1261–1267.

[10] Z. Qiao, Z. Wang, C. Zhang, S. Yuan, Y. Zhu, J. Wang, S. Wang, PVAm–PIP/PS composite membrane with high performance for CO_2/N_2 separation, AIChE J. 59 (2013) 215–228.

[11] Y. Chen, B. Wang, L. Zhao, P. Dutta, W.S. Winston Ho, New Pebax®/zeolite Y composite membranes for CO_2 capture from flue gas, J. Membr. Sci. 495 (2015) 415–423.

[12] Y. Chen, W.S.W. Ho, High-molecular-weight polyvinylamine/piperazine glycinate membranes for CO_2 capture from flue gas, J. Membr. Sci. 514 (2016) 376–384.

[13] W. Salim, V. Vakharia, Y. Chen, D. Wu, Y. Han, W.S.W. Ho, Fabrication and field testing of spiral-wound membrane modules for CO_2 capture from flue gas, J. Membr. Sci. 556 (2018) 126–137.

[14] Y. Han, W. Salim, K.K. Chen, D. Wu, W.S.W. Ho, Field trial of spiral-wound facilitated transport membrane module for CO_2 capture from flue gas, J. Membr. Sci. 575 (2019) 242–251.

[15] Y. Zhao, W.S.W. Ho, Steric hindrance effect on amine demonstrated in solid polymer membranes for CO_2 transport, J. Membr. Sci. 415–416 (2012) 132–138.

[16] L. Deng, T.J. Kim, M.B. Hagg, Facilitated transport of CO_2 in novel PVAm/PVA blend membrane, J. Membr. Sci. 340 (2009) 154–163.

[17] C. Yi, Z. Wang, M. Li, J. Wang, S. Wang, Facilitated transport of CO_2 through polyvinylamine/polyethylene glycol blend membranes, Desalination 193 (2006) 90–96.

[18] Y. Chen, L. Zhao, B. Wang, P. Dutta, W.S.W. Ho, Amine-containing polymer/zeolite Y composite membranes for CO_2/N_2 separation, J. Membr. Sci. 497 (2016) 21–28.

[19] D. Wu, Y. Han, W. Salim, K.K. Chen, J. Li, W.S.W. Ho, Hydrophilic and morphological modification of nanoporous polyethersulfone substrates for composite membranes in CO_2 separation, J. Membr. Sci. 565 (2018) 439–449.

[20] R. Pang, K.K. Chen, Y. Han, W.S.W. Ho, Highly permeable polyethersulfone substrates with bicontinuous structure for composite membranes in CO_2/N_2 separation, J. Membr. Sci. 612 (2020) 118443.

[21] R.J. Young, P.A. Lovell, Introduction to Polymers: Third Edition, CRC Press, Boca Raton, FL, USA, 2011.

[22] J.W. Vanderhoff, E.B. Bradford, H.L. Tarkowski, J.B. Shaffer, R.M. Wiley, Polymerization and Polycondensation Processes, American Chemical Society, 1962.

[23] T.W. Lai, B.R. Vijayendran, Compositions containing high molecular weight poly(vinylamines) for enhanced oil recovery, U.S. Patent 4,798,871, 1989.

[24] P.J. Flory, Principles of Polymer Chemistry, Cornell University Press, Ithaca, N. Y., 1953.

[25] Y. Han, D. Wu, W.S.W. Ho, Nanotube-reinforced facilitated transport membrane for CO_2/N_2 separation with vacuum operation, J. Membr. Sci. 567 (2018) 261–271.

[26] R.K. Pinschmidt, W.L. Renz, W.E. Carroll, K. Yacoub, J. Drescher, A.F. Nordquist, N. Chen, N-Vinylformamide - Building block for novel polymer structures, J. Macromol. Sci. - Pure Appl. Chem. A34 (1997) 1885–1905.

[27] L. Gu, S. Zhu, A.N. Hrymak, Acidic and basic hydrolysis of poly(N-vinylformamide), J. Appl. Polym. Sci. 86 (2002) 3412–3419.

[28] E. Witek, M. Pazdro, E. Bortel, Mechanism for base hydrolysis of poly(N-vinylformamide), J. Macromol. Sci., Part A: Pure Appl. Chem. 44 (2007) 503–507.

[29] Z. Tong, W.S.W. Ho, New sterically hindered polyvinylamine membranes for CO_2 separation and capture, J. Membr. Sci. 543 (2017) 202–211.

[30] E.J. Singley, A. Daniel, D. Person, E.J. Beckman, Determination of Mark-Houwink parameters for poly(N-vinylformamide), J. Polym. Sci., Part A: Polym. Chem. 35 (1997) 2533–2534.

[31] A. Bondi, Van der Waals Volumes and Radii, J. Phys. Chem. 68 (1964) 441–451.

[32] S. Sugden, Molecular volumes at absolute zero. Part II. Zero volumes and chemical composition, J. Chem. Soc. (1927) 1786–1798.

[33] D. Wu, Y. Han, L. Zhao, W. Salim, V. Vakharia, W.S.W. Ho, Scale-up of zeolite-Y/polyethersulfone substrate for composite membrane fabrication in CO_2 separation, J. Membr. Sci. 562 (2018) 56–66.

[34] Y. Han, D. Wu, W.S.W. Ho, Simultaneous effects of temperature and vacuum and feed pressures on facilitated transport membrane for CO_2/N_2 separation, J. Membr. Sci. 573 (2018) 476–484.

[35] H. Ni, K. Debelak, D. Hunkeler, Temperature control of highly exothermic batch polymerization reactors, J. Appl. Polym. Sci. 63 (1997) 761–772.

[36] L. Gu, S. Zhu, A.N. Hrymak, R.H. Pelton, Kinetics and modeling of free radical polymerization of N-vinylformamide, Polymer 42 (2001) 3077–3086.

[37] S. Yu, M. Ma, J. Liu, J. Tao, M. Liu, C. Gao, Study on polyamide thin-film composite nanofiltration membrane by interfacial polymerization of polyvinylamine (PVAm) and isophthaloyl chloride (IPC), J. Membr. Sci. 379 (2011) 164–173.

[38] J.M. Zhu, C. Gosen, R.E. Marchant, Synthesis and characterization of poly(vinyl amine)-based amphiphilic comb-like dextran glycopolymers by a two-step method, J. Polym. Sci., Part A: Polym. Chem. 44 (2006) 192–199.

[39] X. Chen, Y. Wang, R. Pelton, pH-dependence of the properties of hydrophobically modified polyvinylamine, Langmuir 21 (2005) 11673–11677.

[40] J. Xu, R. Pelton, A new route to poly(N-isopropylacrylamide) microgels supporting a polyvinylamine corona, J. Colloid Interface Sci. 276 (2004) 113–117.

[41] M.B. Ahmad, M.B. Huglin, DSC studies on states of water in crosslinked poly(methyl methacrylate-co-n-vinyl-2-pyrrolidone) hydrogels, Polym. Int. 33 (1994) 273–277.

[42] T. Tran, C. Lin, S. Chaurasia, H. Lin, Elucidating the relationship between states of water and ion transport properties in hydrated polymers, J. Membr. Sci. 574 (2019) 299–308.

[43] R. Casadei, D. Venturi, M.G. Baschetti, L. Giorgini, E. Maccaferri, S. Ligi, Polyvinylamine membranes containing graphene-based nanofillers for carbon capture applications, Membranes 9 (2019) 20.

[44] M. Le Berre, Y. Chen, D. Baigl, From convective assembly to Landau-Levich deposition of multilayered phospholipid films of controlled thickness, Langmuir 25 (2009) 2554–2557.

[45] X. Gu, L. Shaw, K. Gu, M.F. Toney, Z. Bao, The meniscus-guided deposition of semiconducting polymers, Nat. Commun. 9 (2018) 16.

[46] L. Ansaloni, Y. Zhao, B.T. Jung, K. Ramasubramanian, M. Giacinti Baschetti, W.S.W. Ho, Facilitated transport membranes containing amino-functionalized multi-walled carbon nanotubes for high-pressure CO_2 separations, J. Membr. Sci. 490 (2015) 18–28.

[47] D.W. Breck, Zeolite Molecular Sieves: Structure, Chemistry, and Use, Wiley, New York, 1973.

[48] G.C. Eastmond, P.C.B. Page, J. Paprotny, R.E. Richards, R. Shaunak, Molecular-weight dependence of gas-permeability and selectivity in copolyimides, Polymer 34 (1993) 667–670.

[49] X. Deng, C. Zou, Y. Han, L.-C. Lin, W.S.W. Ho, Computational evaluation of carriers in facilitated transport membranes for postcombustion carbon capture, J. Phys. Chem. C 124 (2020) 25322–25330.

Figure captions

Fig. 1. Schematic of inverse emulsion polymerization.

Fig. 2. Schematic of PVAm synthesis from NVF.

Fig. 3. Mark-Houwink plot of PNVF synthesized with IEP.

Fig. 4. Effect of monomer concentration on MW of PNVF. 0.019 wt.% initiator and 70ºC reaction temperature.

Fig. 5. Effect of initiator concentration on MW of PNVF. 42.5 wt.% monomer and 70ºC reaction temperature.

Fig. 6. Effect of reaction temperature on MW of PNVF. 0.019 wt.% initiator and 42.5 wt.% monomer.

Fig. 7. NMR spectra of (a) PNVF and (b) PVAm·HCl.

Fig. 8. Effect of HCl/amide ratio on the DOH of PVAm at 75ºC.

Fig. 9. TGA and DTG curves of PVAm with MW of 12.7 MDa.

Fig. 10. Effect of PVAm MW on transport performances of neat PVAm membranes.

Fig. 11. Effect of PVAm MW on coating solution viscosity and thickness of selective layer. The trendlines are for the guide of eyes.

Fig. 12. UV–Vis absorbance of 2 wt.% PVAm polymer solutions with different MWs. The trendline is for the guide of eyes.

Fig. 13. Effect of the DOH of PVAm on transport performances of neat PVAm membranes. The trendlines are for the guide of eyes.

Fig. 14. Effect of the DOH of PVAm on transport performances of PVAm/PG (35/65 by wt.) membranes. The trendlines are for the guide of eyes.

Fig. 15. Effect of the DOH of PVAm on V, V_0, and FFV of PVAm/PG (35/65 by wt.) membranes. The trendlines are for the guide of eyes.

Fig. 16. Effect of PG content on membrane transport performances.

Fig. S1. Berry plot for determining the weight-average MW of a PVNF sample with a MW of 14.3 MDa.

Fig. S2. SEM images of PVAm/PG (35/65 by wt.) membranes with PVAm MWs of (a) 5.2, (b) 11.2, (c) 12.7 and (d) 14.3 MDa.